Optik 124 (2013) 1601–1608

Contents lists available at SciVerse ScienceDirect

Optik

journal homepage: www.elsevier.de/ijleo

Hyperspectral and panchromatic image fusion using unmixing-based constrained nonnegative matrix factorization☆

Zhou Zhang[a], Zhenwei Shi[a,b,c,*], Zhenyu An[a]

[a] Image Processing Center, School of Astronautics, Beihang University, Beijing 100191, P.R. China
[b] Beijing Key Laboratory of Digital Media, Beihang University, Beijing 100191, P.R. China
[c] State Key Laboratory of Virtual Reality Technology and Systems, Beihang University, Beijing 100191, P.R. China

ARTICLE INFO

Article history:
Received 27 December 2011
Accepted 29 April 2012

Keywords:
Hyperspectral image fusion
Spectra unmixing
Constrained nonnegative matrix factorization (CNMF)
Projected gradient algorithm

ABSTRACT

Image fusion is an important technique in remote sensing, as it could effectively combine the high spatial and the high spectral resolutions in order to obtain the complete and accurate description of the observed scene. To date, many image fusion techniques have been developed. However, the available methods could hardly produce the satisfactory results in dealing with the fusion between the hyperspectral image and panchromatic image, especially in the spectral aspect. Therefore, in this paper, a new fusion approach, called unmixing-based constrained nonnegative matrix factorization (UCNMF), is proposed. This approach uses the NMF unmixing technique to generate the abundance matrix and uses the panchromatic image to sharpen the the material maps. The constrained term aiming at preserving the spectral information is added and the fusion problem is turned into a constrained optimization problem. Additionally, a projected gradient algorithm aiming at get the numerical solution of the optimization problem is presented. Finally, three groups of experiments are given to demonstrate that the proposed fusion method could be recognized as an effective technique in hyperspectral image fusion.

1. Introduction

Hyperspectral remote sensing is a significant technique that has been used in many applications, such as ground-objects classification, mineral exploration and identification of natural and man-made materials [24]. The hyperspectral images, taken from the satellites or the airplanes, have two spatial dimensions and one spectral dimension [19]. In many cases, the hyperspectral images keep good spectral feature while low spatial resolution. In contrast, the panchromatic image has high spatial resolution, but it has limitations in spectral character. Hence, in order to obtain the fused images with both high spectral and spatial resolutions, researches aim at proposing fusion techniques for integrating different kinds of images have developed.

Because of the importance of image fusion techniques, several algorithms have been proposed. These techniques are usually divided into two groups [32]: spectral component substitution techniques, such as the intensity, hue and saturation (IHS) transform [4,25]; spatial domain techniques, such as the high-pass filtering (HPF) [2,31]. The base concept of IHS method is replacing the intensity component of the low spatial resolution image with the panchromatic image. In practical applications, IHS is widely used because of its fast computing ability [11]. However, the intensity band and the panchromatic band often differ from each other to a certain extend and thus the color distortion becomes a common problem of the IHS technique [7,21]. In order to preserve the spectral information, the HPF method only transfers the excess high spatial frequency components into all the spectral bands with low spatial resolution. Compared to the IHS method, HPF could reduce the degree of spectral distortion. However, HPF would also cause spectral distortion for the reason that the detailed information extracted from the panchromatic image differs from the existing information in the original hyperspectral image.

Spectral unmixing is a technique that could estimate the percentage of each material (called endmembers) within each low resolution hyperspectral pixel [1]. The output of spectral unmixing is the fraction maps of the endmembers at the spatial resolution of the hyperspectral system. Through the unmixing process, we could know the endmembers and their abundances in the images. Recently, many hyperspectral unmixing techniques have been

☆ The work was supported by the National Natural Science Foundation of China under the Grants 60975003 and 91120301,the 973 Program under the Grant 2010CB327904, the open funding project of State Key Laboratory of Virtual Reality Technology and Systems, Beihang University (Grant No. BUAA-VR-12KF-07), the Fundamental Research Funds for the Central Universities under the Grants YWF-10-01-A10 and YWF-11-03-Q-066, the Beijing Natural Science Foundation (Non-negative Component Analysis for Hyperspectral Imagery Unmixing) under the Grant 4112036, and Program for New Century Excellent Talents in University of Ministry of Education of China under the Grant NCET-11-0775.

* Corresponding author. Tel.: +86 10 823 16 502; fax: +86 10 823 38 798.
E-mail address: shizhenwei@buaa.edu.cn (Z. Shi).

0030-4026/$ – see front matter © 2012 Elsevier GmbH. All rights reserved.
http://dx.doi.org/10.1016/j.ijleo.2012.04.022

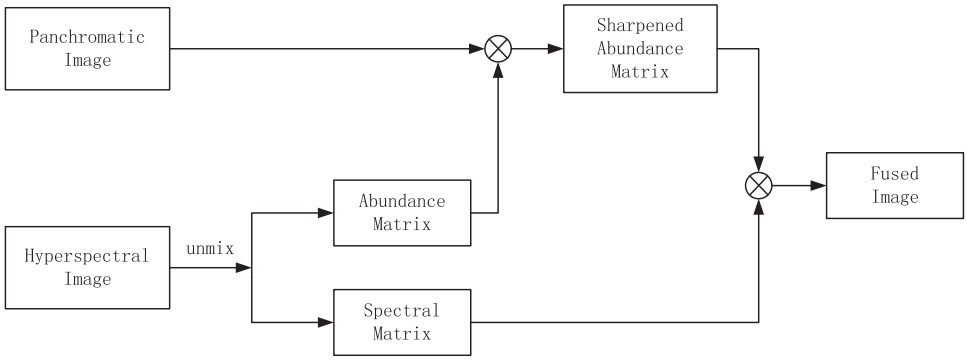

Fig. 1. Proposed fusion process.

developed based on a linear spectral mixture model [13,16,20]. Many of them are convex-geometry-based approaches, the limitation of this kind of method is that the assumption of one pure pixel for each endmember is needed [3,20]. Nonnegative matrix factorization (NMF), which was first proposed by Lee and Seung [17] has been applied to hyperspectral unmixing [15]. To unmix hyperspectral data, the image cube is decomposed into the spectral matrix and the abundance matrix by using the NMF technique without the pure pixel assumption.

In this paper, we propose an unmixing-based constrained NMF (UCNMF) model for hyperspectral and panchromatic data fusion. In the fusion, the abundance matrix is obtained via unmixing and its spatial resolution is enhanced by making the fusion with the high spatial resolution image (panchromatic image). Taking into account of the necessary of the spectral-preservation, a regularized term is added based on the original NMF. Therefore, as a whole, fused data with both high spatial and spectral resolutions could be generated. The reconstruction qualities are evaluated by three groups of experiments including both synthetic data and real data. Comparison results with IHS and HPF are also provided.

This paper is organized as follows. Section 2 describes the UCNMF model for the hyperspectral and panchromatic data fusion. Section 3 uses the projected gradient algorithm to get the numerical solution of the proposed model. Section 4 gives the experimental results of different fusion methods and finally close with conclusions in Section 5.

2. Unmixing-based constrained nonnegative matrix factorization (UCNMF) fusion model

The aim of the hyperspectral image fusion is to produce the fused image with high spatial and spectral resolutions simultaneously. To conduct the fusion model, these two requirements should be considered.

2.1. Nonnegative matrix factorization (NMF) for hyperspectral unmixing

The hyperspectral data is a 3D-array data and we use a 2D-array matrix $\mathbf{V} \in \mathbb{R}^{L\times K}$ to store the original hyperspectral data. Where L and K represents the number of bands and pixels, respectively. Each row of $\mathbf{V}$ stands for one band of the original hyperspectral image. In dealing with the unmixing problem, a linear spectral mixture model is commonly used. At each pixel, a spectrum is assumed to be a linear combination of several endmember spectra. Therefore, $\mathbf{V}$ could be represented as

$$\mathbf{V} = \mathbf{WH} + \mathbf{N} \tag{1}$$

where $\mathbf{W} \in \mathbb{R}^{L\times S}$ is the spectral signature matrix, with each column $\{\mathbf{w}_r\}_{r=1}^{P} \in \mathbb{R}^{L}$ representing the endmember spectrum (the spectrum of a pure object, such as tree, rive, and roof) and S representing the number of endmembers (the pure objects). $\mathbf{H} \in \mathbb{R}^{S\times K}$ is the abundance matrix, with each column $\{\mathbf{h}_j\}_{j=1}^{K} \in \mathbb{R}^{S}$ representing the fractions of all the endmembers at a certain pixel. $\mathbf{N}$ is the noise item with the property of indeterminacy.

To unmix the hyperspectral data, NMF could be conducted by minimization the square of the Euclidean distance [18] between $\mathbf{V}$ and $\mathbf{WH}$ as follows:

$$Euc(\mathbf{W},\mathbf{H}) = \frac{1}{2}\|\mathbf{V}-\mathbf{WH}\|^2 = \frac{1}{2}\sum_i\sum_j(\mathbf{V}_{ij}-(\mathbf{WH})_{ij})^2 \tag{2}$$

2.2. Unmixing-based constrained nonnegative matrix factorization (UCNMF) for image fusion

The proposed fusion model is designed to satisfy the two fusion requirements: high spatial and spectral resolutions. The detail of how to achieve these two purposes are illustrated below, respectively.

Fig. 1 is a graphical depiction of the process of the spatial resolution enhancement. We extend the spectral unmixing approach to make the fusion. First, the spectral unmixing using the NMF technique operates on the original hyperspectral image to create the abundance matrix. The abundance matrix, as mentioned before, represents the fractions of the endmembers at the resolution of the hyperspectral image. Then the image fusion was accomplished by using the panchromatic image to increase the spatial resolution of the abundance matrix. The weighted fusion method, which is a common method in the pixel level, is adopted. According to this, one part of the fusion model aiming at advancing the spatial resolution could be expressed as follows:

$$\begin{aligned} &\min \quad F(\mathbf{W},\mathbf{H}) = \frac{1}{2}\|\mathbf{V}-\mathbf{WH}\|^2 \\ &\text{s.t.} \quad \mathbf{W}\geq 0, \mathbf{H}\geq 0 \end{aligned} \tag{3}$$

Therefore, we have the fused data $\mathbf{V}_f$:

$$\mathbf{V}_f = \mathbf{W}(\alpha\mathbf{H} + (1-\alpha)\mathbf{P}) \tag{4}$$

where $\mathbf{P} \in \mathbb{R}^{S\times K}$ represents replication of the panchromatic data. Each row of $\mathbf{P}$ denotes the panchromatic image and there are totally S times of replications. α is the weighed coefficient.

On the other hand, we should also consider how to preserve the spectral information of the original hyperspectral image. In the proposed fusion model, the spatial detail information of the panchromatic image is added to the fused image. However, this part of information does not hold the same spectral quality with that of the original hyperspectral image. As a result, after the reconstruction, the spectral information of the fused image differs from that of the original hyperspectral image and thus the spectral distortion happens. To overcome this problem, we try to find a

regularized term to constrain the spectral difference between the original hyperspectral image and the fused image.

Spectral angle mapper (SAM) [26] is an important assessment for the spectral dimension of the hyperspectral data, which is defined as SAM = $\arccos((\langle \mathbf{a}, \mathbf{b}\rangle)/(\|\mathbf{a}\|\|\mathbf{b}\|))$, where $\mathbf{a}, \mathbf{b}$ respectively represents the certain pixel's spectral vector before and after the fusion. The smaller the value of the SAM is, the better the performance of the spectral preservation has. Hence, SAM can be a useful constraint function to refrain from spectral distortion. In this paper, each pixel's SAM is defined as:

$$\mathrm{SAM} = \arccos\left(\frac{\langle \mathbf{v}_{fi}, \mathbf{v}_i\rangle}{\|\mathbf{v}_{fi}\|\|\mathbf{v}_i\|}\right) \tag{5}$$

where $\mathbf{v}_{fi} \in \mathbb{R}^L$ is the ith column of the fused data $\mathbf{V}_f$ and i represents the ith pixel in the image. Similarly, $\mathbf{v}_i$ represents the ith column of the original hyperspectral data and it has the same size with $\mathbf{v}_{fi}$. Then, we can calculate the sum of all the pixels' SAM:

$$\mathrm{SAM\_sum} = \sum_{i=1}^{K} \arccos\left(\frac{\langle \mathbf{v}_{fi}, \mathbf{v}_i\rangle}{\|\mathbf{v}_{fi}\|\|\mathbf{v}_i\|}\right) \tag{6}$$

where K represents the number of the pixels. Consider that the anti trigonometric function in (6) is difficult to be implemented and we can simplify it by just using its cosine value instead. Therefore, we have:

$$\mathrm{SAM\_sum\_cos} = \sum_{i=1}^{K} \left(\frac{\langle \mathbf{v}_{fi}, \mathbf{v}_i\rangle}{\|\mathbf{v}_{fi}\|\|\mathbf{v}_i\|}\right) \tag{7}$$

To do the further simplification, we use the substraction instead of the division and the quadratic style of (7) is chosen, then we have:

$$S(\mathbf{V}_f) = \sum_{i=1}^{K} (\|\mathbf{v}_{fi}\|^2\|\mathbf{v}_i\|^2 - \langle \mathbf{v}_{fi}, \mathbf{v}_i\rangle^2) \tag{8}$$

However, it is still not convenient for us to directly use (8) as the constraint function in the calculation and we transform it into the following formation, which is equivalent to (8).

$$S(\mathbf{V}_f) = tr((\mathbf{V}_f^T\mathbf{V}_f)\cdot*(\mathbf{V}^T\mathbf{V})) - tr((\mathbf{V}_f^T\mathbf{V}).*(\mathbf{V}_f^T\mathbf{V})) \tag{9}$$

where $\cdot*$ is the elementwise product, $(\cdot)^T$ denotes the transposition of the matrix and $tr(\cdot)$ represents the trace of the matrix. The function (9) is recognized as the final spectral constraint function. Adding (9) into the model (3) then we obtain the final fusion model:

$$\begin{aligned} &\min \quad J(\mathbf{W}, \mathbf{H}) = F(\mathbf{W}, \mathbf{H}) + \beta S(\mathbf{V}_f) \\ &\text{s.t.} \quad \mathbf{W} \geq 0, \mathbf{H} \geq 0 \end{aligned} \tag{10}$$

where β is a constant weight which is used to keep a balance between the spectral quality and the spatial quality of the fused image. $F(\mathbf{W}, \mathbf{H})$ is defined in (3) and $S(\mathbf{V}_f)$ is defined in (9). Finally, we obtain the fused data

$$\mathbf{V}_f = \mathbf{W}(\alpha\mathbf{H} + (1-\alpha)\mathbf{P}) \tag{11}$$

This new proposed model improves the image's spatial resolution by using the panchromatic image $\mathbf{P}$. Simultaneously, the spectral character can be well preserved by the spectral constraint function $S(\mathbf{V}_f)$. In Section 3, we will discuss how to solve the optimization problem in (10) and (11).

3. Projected gradient algorithm for UCNMF

The proposed fusion model is a bound-constrained optimization problem. To solve this problem, the projected gradient method (PG) is a simple and effective one among the existing techniques. Some researchers have used PG algorithm to deal with the NMF problem [5,14,18,30]. Among these PG algorithms, the Lin-PG NMF algorithm is widely used and well known for NMF problems [30]. Lin applied projected gradient method to NMF directly with working on the whole matrices $\mathbf{W}$ and $\mathbf{H}$, rather than their individual columns. To apply the Lin-PG algorithm to our fusion model (10) and (11), the gradient of the function $J(\mathbf{W}, \mathbf{H})$ should be obtained first. We have:

$$\begin{aligned} \nabla_{\mathbf{W}} J(\mathbf{W}, \mathbf{H}) = {} & (\mathbf{W}\mathbf{H} - \mathbf{V})\mathbf{H}^T + 2\beta\mathbf{W}\mathbf{H}_0 diag(\mathbf{V}^T\mathbf{V})\mathbf{H}_0^T \\ & - 2\beta\mathbf{V} diag(\mathbf{H}_0^T\mathbf{W}^T\mathbf{V})\mathbf{H}_0^T \end{aligned} \tag{12}$$

$$\begin{aligned} \nabla_{\mathbf{H}} J(\mathbf{W}, \mathbf{H}) = {} & \mathbf{W}^T(\mathbf{W}\mathbf{H} - \mathbf{V}) + 2\beta\alpha^2\mathbf{W}^T\mathbf{W}\mathbf{H} diag(\mathbf{V}^T\mathbf{V}) + 2\beta\alpha(1-\alpha) \\ & \mathbf{W}^T\mathbf{W}\mathbf{P} diag(\mathbf{V}^T\mathbf{V}) - 2\beta\alpha^2\mathbf{W}^T\mathbf{V} diag(\mathbf{H}^T\mathbf{W}^T\mathbf{V}) \\ & - 2\beta(1-\alpha)^2\mathbf{W}^T\mathbf{V} diag(\mathbf{P}^T\mathbf{W}^T\mathbf{V}) \end{aligned} \tag{13}$$

where $(\cdot)^T$ represents the transposition of the matrix. $\mathbf{H}_0 = \alpha\mathbf{H} + (1-\alpha)\mathbf{P}$. $diag(*)$ is a diagonal matrix made up from the diagonal elements in matrix $*$.

From the current solution $\mathbf{W}^k, \mathbf{H}^k$, both matrices could be simultaneously updated to $\mathbf{W}^{k+1}, \mathbf{H}^{k+1}$:

$$\mathbf{W}^{k+1} = P_\Omega[\mathbf{W}^k - \gamma_k \nabla_{\mathbf{W}} J(\mathbf{W}^k, \mathbf{H}^k)] \tag{14}$$

$$\mathbf{H}^{k+1} = P_\Omega[\mathbf{H}^k - \gamma_k \nabla_{\mathbf{H}} J(\mathbf{W}^k, \mathbf{H}^k)] \tag{15}$$

where $P_\Omega[\xi]$ is a projection of $[\xi]$ and it could maps the point back to the bounded feasible region [18]. In the NMF problem, the projection $P_\Omega[\xi]$ could be performed in the way of replacing all negative elements in ξ by zero-values.

Different projected gradient methods differs on selecting the learning parameter γ_k. Lin considers a simple and effective one called "Armiyo rule along the projection arc". γ_k could be decided by:

$$\gamma_k = \lambda^{t_k} \tag{16}$$

where $\lambda \in (0, 1)$ and t_k is the first non-negative integer t for which

$$\begin{aligned} J(\mathbf{W}^{k+1}, \mathbf{H}^{k+1}) - J(\mathbf{W}^k, \mathbf{H}^k) \leq {} & \sigma(\nabla_{\mathbf{W}} J(\mathbf{W}^k, \mathbf{H}^k)^T(\mathbf{W}^{k+1} - \mathbf{W}^k) \\ & + \nabla_{\mathbf{H}} J(\mathbf{W}^k, \mathbf{H}^k)^T(\mathbf{H}^{k+1} - \mathbf{H}^k)) \end{aligned} \tag{17}$$

where $\sigma \in (0, 1)$. For NMF, the stopping condition given by Lin is the following:

$$\|\nabla^P J(\mathbf{W}^k, \mathbf{H}^k)\|_F \leq \varepsilon \|\nabla J(\mathbf{W}^1, \mathbf{H}^1)\|_F \tag{18}$$

where $\varepsilon \in (0, 1)$, $\|\cdot\|_F$ is the Frobenius norm and $\nabla^P f(\mathbf{W}^k, \mathbf{H}^k)$ is the projected gradient.

Algorithm *(Outline: Lin-PG for UCNMF).*

1. Given $0 < \delta < 1, 0 < \sigma < 1, 0 < \varepsilon < 1$. Set $\gamma_0 = 1$.
   Initialize the matrices $\mathbf{W} \geq \mathbf{0}, \mathbf{H} \geq \mathbf{0}$. Calculate the $\|\nabla J(\mathbf{W}^1, \mathbf{H}^1)\|_F$.
2. For k = 1, 2, ...
   (a) Assign $\gamma_k \longleftarrow \gamma_{k-1}$.
   (b) If γ_k satisfies (17), repeatedly increase it by $\gamma_k \longleftarrow \gamma_k/\delta$
   until either γ_k does not satisfy (17)
   or $\mathbf{W}, \mathbf{H}$ keep the same before and after the change of γ_k
   Else repeatedly decrease γ_k by $\gamma_k \longleftarrow \gamma_k \cdot \delta$
   until γ_k satisfies (17).
   (c) Update $\mathbf{W}$ by (14), $\mathbf{H}$ by (15).
   (d) Calculate the $\|\nabla^P J(\mathbf{W}^k, \mathbf{H}^k)\|_F$.
3. Repeat step 2, until satisfying the stopping condition given in (18).
4. Obtaining the fused image $\mathbf{V}_f$ by $\mathbf{V}_f = \mathbf{W}(\alpha\mathbf{H} + (1-\alpha)\mathbf{P})$.

4. Experimental results and analysis

In this section, three experiments including one group of synthetic hyperspectral image and two groups of real hyperspectral

images are conducted. In each group of experiment, the proposed UCNMF algorithm is compared to other two popular methods: IHS and HPF. The parameters we choose for the UCNMF is $\beta = 10^{-3}$, $\alpha = 0.5, \delta = 0.1, \sigma = 0.01, \varepsilon = 0.001$. Six image quality metrics are listed here in order to make an objective evaluation.

4.1. Performance evaluation

One possible approach to evaluate the performance of the proposed algorithm is that examine the images visually in a qualitative manner. However, this kind of evaluation may rely on people too much and thus quantitative measures are necessary to be employed. The result of the fused images can be evaluated from two points: the spatial resolution of each spectral band image and the spectral quality of each spectrum at a single pixel [22]. Six typical metrics are introduced below.

4.1.1. Entropy (E)

The entropy [8,23] of an image is given by

$$E = -\sum_{l=1}^{N} P(d_i) log_2(P(d_i)) \tag{19}$$

where d_i denotes the possible gray value in the image and $p(d_i)$ is the probability of that particular gray value. Entropy reflects the amount of information of the image. High entropy value reflects the high spatial resolution of the image.

4.1.2. Spectral angle mapper (SAM)

SAM is defined in expression (5), which has been widely used in hyperspectral image analysis to measure the spectral similarity between the fused image and the original hyperspectral image. In this paper, we use (5) to calculate the sum of all the pixels' SAM, and compute its mean value as the final SAM. Therefore, SAM could be recognized as a global measurement of spectral distortion and small angle indicates high similarity [11].

4.1.3. Correction coefficient (CC)

CC [28] is defined as:

$$\mathrm{CC} = \frac{\sum_{x=1}^{M}\sum_{y=1}^{N}[A(x,y) - \overline{A(x,y)}][B(x,y) - \overline{B(x,y)}]}{\sqrt{\sum_{x=1}^{M}\sum_{y=1}^{N}[A(x,y) - \overline{A(x,y)}]^2 \sum_{x=1}^{M}\sum_{y=1}^{N}[B(x,y) - \overline{B(x,y)}]^2}} \tag{20}$$

where $A(x, y)$ and $B(x, y)$ represent the gray value of the pixel at the location of (x, y) in two images. $\overline{A(x,y)}$ and $\overline{B(x,y)}$ represents the mean gray value of all the pixels in image A and B, respectively. CC could be used to evaluate the correlative degree of the fused image and the original hyperspectral image. The higher the value is, the better the spectral quality of the fused image has. Its perfect value is 1.

4.1.4. Spectral information divergence (SID)

SID could be used to describe the statistic of a spectrum, which could show the spectral closeness between the fused and the original hyperspectral images at a pixel level [6]. Ideally, it should be close to zero. To compute SID, we have the vector $\mathbf{x} = (x_1, \ldots, x_N)^T$, which is taken from the original hyperspectral image and $\mathbf{y} = (y_1, \ldots, y_N)^T$, which is a vector from the final fused image. Then we have

$$p_j = \frac{x_j}{\sum_{i=1}^{N} x_i} \tag{21}$$

$$q_j = \frac{y_j}{\sum_{i=1}^{N} y_i} \tag{22}$$

where N is the number of bands. We define SID as:

$$\mathrm{SID} = D(x\|y) + D(y\|x) \tag{23}$$

$D(x \| y)$ and $D(y \| x)$ are defined as follows:

$$D(x\|y) = \sum_{i=1}^{L} p_i \log\left(\frac{p_i}{q_i}\right) \tag{24}$$

$$D(y\|x) = \sum_{i=1}^{K} p_i \log\left(\frac{p_i}{q_i}\right) \tag{25}$$

where N and K are the bands when p_i, q_i are not equal to zero.

4.1.5. Q-average (Q)

The metric of the Q is defined as follows:

$$Q = \frac{4\sigma_{xy}\bar{x}\bar{y}}{(\sigma_x^2 + \sigma_y^2)[(\bar{x}^2) + (\bar{y}^2)]} \tag{26}$$

where $\bar{x}$ and $\bar{y}$ represent the average gray values of images x and y, respectively. σ_x and σ_y are the variances of images x and y respectively. σ_{xy} is defined as $(1/N-1)\sum_{i=1}^{N}(x_i - \bar{x})(y_i - \bar{y})$. Q-average reflects the integration of three aspects: "loss of correlation, luminance distortion, and contrast distortion"[10] and its perfect value is one.

4.1.6. Relative dimensionless global error in synthesis (ERGAS)

The metric of the ERGAS is defined as follows:

$$\mathrm{ERGAS} = 100\frac{h}{l}\sqrt{\frac{1}{L}\sum_{i=1}^{L}\frac{\mathrm{RMSE}_i^2}{\mu_i^2}} \tag{27}$$

where h is the resolution of panchromatic image, l is the resolution of the hyperspectral image, μ_i is the mean radiance of each spectral band, L is the number of bands. RMSE is the root mean square error defined as follows [10]:

$$\mathrm{RMSE} = \sqrt{\frac{1}{MN}\sum_{x=1}^{M}\sum_{y=1}^{N}(S(x,y) - F(x,y))^2} \tag{28}$$

where $S(x, y)$ and $F(x, y)$ are the standard and fused image, respectively. The value of ERGAS denotes the difference between the two images and it is expected to be zero.

4.2. Synthetic image experiment

In this experiment, the synthetic data was generated from the real airbone hyperspectral data. The real hyperspectral image was taken over an urban scene in Texas by the hyperspectral digital imagery collection experiment (HYDICE) sensor, which contains 210 bands with the spectral resolution of 10 nm acquired in the 400–2400 nm region. We obtained the data from the internet [27] with 1–100 bands and selected the subscene with the size of 307×306. First, we chose the image of band 4 as the panchromatic image for it had a comparative higher spatial resolution. Second, the original hyperspectral data was down sampled by a factor of 4 and was resized using the the bilinear interpolation to make it has the same size as before. In this manner, the panchromatic image and the hyperspectral image have a fourfold difference in spatial resolution and both images were geometrically registered before the fusion.

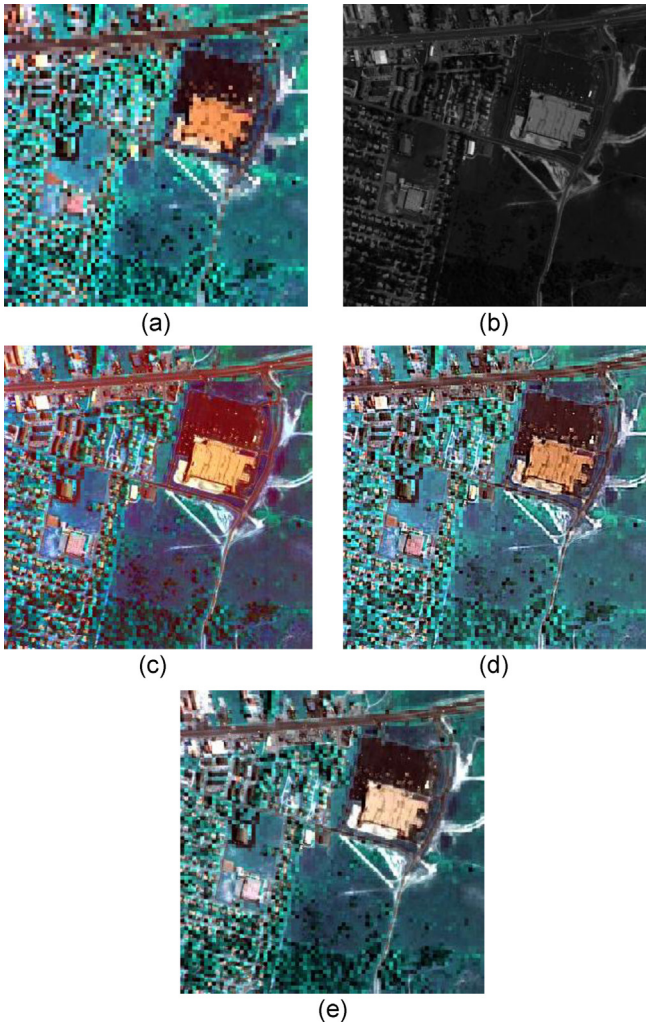

Fig. 2. Original images and fused images by using different methods: (a) Original hyperspectral image, (b) panchromatic image, (c) fused image by IHS, (d) fused image by HPF, and (e) fused image by UCNMF. (For interpretation of the references to color in the text, the reader is referred to the web version of the article.)

4.2.1. Visual analysis

The original hyperspectral image, the panchromatic image and the fused images yielded by different methods are shown in false color with band 30, 60, 90 in Fig. 2. Fig. 2(a) is the original hyperspectral image. Fig. 2(b) is the panchromatic image. Fig. 2(c)–(e) are the fused images yielded by IHS, HPF and UCNMF method, respectively.

Compared to the original hyperspectral image, these fused images all have better spatial qualities. For example, the buildings, houses and streets could be easily identified after the fusion. However, these three fusion methods perform differently in the spectral aspect. It is obvious that the image obtained by IHS has serious spectral distortion. The whole image presents excessive red (see Fig. 2(c)). The images obtained by HPF and UCNMF appear to have better spectral fidelity.

4.2.2. Statistical analysis

To analyze the performances of previous methods quantitatively, only relying on the visual evaluation is not enough. Therefore, we evaluate them by using the six typical metrics mentioned before. The standard image for this experiment is the hyperspectral image without being down sampled. Table 1 shows the objective metrics for the synthetic image experiment. The bold font is the best one in the same row. From Table 1, it can be found that the fused image yielded by the UCNMF contains the most spatial detailed information because of the highest value of *E*. In term of the spectral fidelity, the image obtained by IHS has the worst values in SAM, CC, SID and *Q*, which are all used to evaluate the spectral performance and this result just accords with the visual evaluation. In the contrary, the proposed method UCNMF has the most desirable values in those metrics. Besides, from the value of ERGAS, we can find that the UCNMF has the best performance among these three methods when considering the integration results of the two aspects: spatial and spectral resolutions.

4.3. Real image experiments

After the synthetic image experiment, we also conducted two groups of real image experiments. In the first experiment, the

Table 1
Objective metrics of synthetic image experiment.

	IHS	HPF	UCNMF
E	6.1909	5.7347	**6.2712**
SAM	14.9162	14.7368	**5.1616**
CC	0.7794	0.8913	**0.9284**
SID	0.2218	0.1669	**0.0259**
Q	0.5769	0.7331	**0.8998**
ERGAS	23.6628	15.7944	**5.9336**

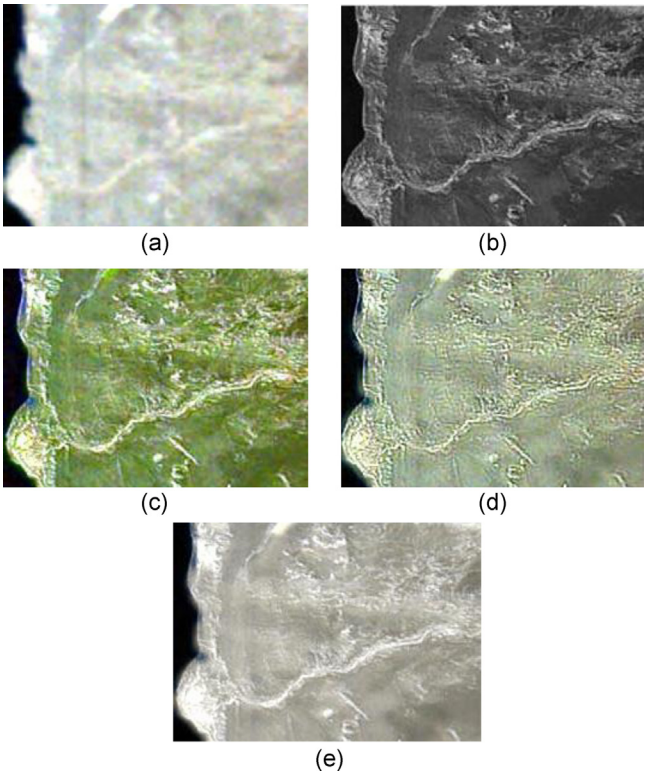

Fig. 3. Original images and fused false color images by using different methods: (a) Original hyperspectral image, (b) panchromatic image, (c) fused image by IHS, (d) fused image by HPF, and (e) fused image by UCNMF. (For interpretation of the references to color in the text, the reader is referred to the web version of the article.)

hyperspectral data was acquired from the HJ1-A satellite, which composed of 110 bands [9] with a spatial solution of 100 m. After removing some bands with low signal-noise-ratio, we used the remaining 100 bands to make the fusion. The corresponding panchromatic image was obtained from the google map [12] with the spatial resolution of 30 m. We selected 256×200 pixel size images for this experiment. In the second experiment, the hyperspectral data was obtained from HYDICE sensor. The subscene from the Washington, DC with the size of 210×270 was selected. There were 64 bands remained after low-SNR bands removed. The corresponding panchromatic image was obtained from the the google map [12] with the spatial resolution of 30 m.

4.3.1. Visual analysis

In the first real image experiment, the original hyperspectral image and fused images are shown in false color with band 10, 40 and 70. In the second real image experiment, these images are shown in false color with band 10, 30 and 50. These bands were chosen randomly. Figs. 3(b) and 4(b) represent the original hyperspectral image. The fused images obtained by the IHS, HPF, UCNMF are shown in Figs. 3(c)–(e) and 4(c)–(e), respectively. From Figs. 3 and 4, the fused images yielded by these three methods seem to be clearer than the original hyperspectral images. Some useful detailed objects, such as the valleys in Fig. 3(c)–(e), the streets and the buildings in Fig. 4(c)–(e) could be recognized with no effort. On the other hand, in term of the spectral fidelity, these three methods perform differently. In the first real image experiment, the fused image obtained by the IHS (Fig. 3(c)) and the HPF (Fig. 3(d)) have turned the original gray image into green. The UCNMF method overcomes the disadvantage of spectral distortion and it has similar color feature with the original hyperspectral image (see Fig. 3(e)). In the second real image experiment, the fused image obtained by the IHS (Fig. 4(c)) and HPF (Fig. 4(d)) also present unnatural color. The IHS method made the whole image have excessive red. The image obtained by HPF has overmuch white color. Only the fused image yielded by the UCNMF (Fig. 4(e)) has good visual quality.

4.3.2. Statistical analysis

Then, we use the objective metrics to make the evaluation as shown in Tables 2 and 3. In the Tables, the bold fond is the best one in the same row. The ERGAS metric is not listed here for the reason that it is impossible for us to find the standard image in the real image experiment. In the spatial aspect, the proposed method UCNMF perform best, which could be demonstrated by the values of E. It indicates that the UCNMF method could inject much detail information from high-resolution image (panchromatic image) into the low-resolution image (hyperspectral image). In the spectral aspect, based on the values of SAM, SID, CC, Q, we can reliably make the conclusion that the proposed method SPNMF has the best spectral quality among these three methods. While the IHS method has the poorest spectral resolution.

4.4. Experimental results analysis

In this paper, we use one group of synthetic data and two groups of real data to conduct the experiments. During the experiments, three fusion methods: IHS, HPF and UCNMF are compared. The results turn out that, these three methods all can improve the spatial resolution of the original hyperspectral image after the fusion process. In term of the spectral preservation, notice that the HPF method performs well in the synthetic experiment while has bad behaviors in the two groups of real image experiments, which reflects that HPF method cannot always satisfy the requirement of high spectral quality in the hyperspectral image fusion. The IHS method causes severe spectral distortion in all the experiments and thus this method is not quite suitable to be used in the hyperspectral image fusion. The proposed method UCNMF has comparatively better performances in these three experiments. Furthermore,

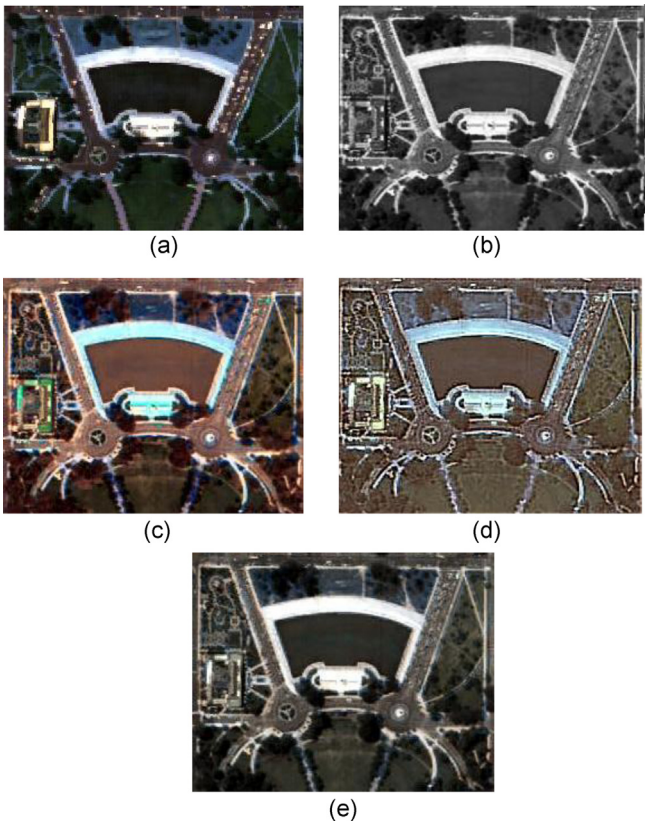

Fig. 4. Original images and fused images by using different methods: (a) Orginal hyperspectral image, (b) panchromatic image, (c) fused image by IHS, (d) fused image by HPF, and (e) fused image by UCNMF. (For interpretation of the references to color in the text, the reader is referred to the web version of the article.)

Table 2
Objective metrics of real image experiment 1.

	IHS	HPF	UCNMF
E	5.7005	5.4655	**5.7596**
SAM	9.5701	9.4524	**3.4129**
CC	0.5104	0.6656	**0.8108**
SID	0.0644	0.0435	**0.0074**
Q	0.4744	0.6102	**0.7903**

Table 3
Objective metrics of real image experiment 2.

	IHS	HPF	UCNMF
E	6.2822	6.2074	**6.8778**
SAM	11.0894	14.6115	**10.9023**
CC	0.6317	0.6825	**0.7483**
SID	0.0656	0.0996	**0.0611**
Q	0.4762	0.5086	**0.5333**

after the evaluations by objective metrics, we could reliably make the conclusion that the proposed method UCNMF could improve the the spatial resolution of the original hyperspectral image and preserve much of the spectral information simultaneously. In general, it is superior to other methods no matter in the synthetic image experiment or in the real image experiments.

5. Conclusions

In this paper, we propose a new model called unmixing-based constrained nonnegative matrix factorization (UCNMF) for the fusion between hyperspectral image and panchromatic image. To get the solution of the fusion model, we change it into a bound-constrained optimization problem and use the projected gradient algorithm, based on the Armijo update rule, to solve the optimization problem. Three experiments including one group of synthetic image experiment and two groups of real image experiment are conducted to evaluate the performances of different methods. The results turn out that, the proposed method UCNMF has the advantage that it could advance the spatial resolution of the hyperspectral image without losing much its color information. As a whole, the UCNMF algorithm has a superior performance over some other traditional methods in dealing with the fusion between hyperspectral image and panchromatic image.

References

[1] J.B. Adams, M.O. Smith, A.R. Gillespie, Imaging spectroscopy: interpretation based on spectral mixture images, Remote Geochem. Anal. Elem. Miner. Compos. 7 (27) (1993) 145–166.
[2] B. Aiazzi, L. Alparone, S. Baronti, A. Garzelli, Context-driven fusion of high spatial and spectral resolution images based on oversampled multi-resolution analysis, IEEE Trans. Geosci. Remote Sens. 40 (10) (2002) 2300–2312.
[3] J.W. Boardman, Geometric mixture analysis of imaging spectrometry data, IEEE Int. Geosci. Remote Sens. Symp. 4 (1994) 2369–2371.
[4] M. Cetin, N. Musaolu, Merging hyperspectral and panchromatic image data: qualitative and quantitative analysis, Int. J. Remote Sens. 30 (7) (2009) 1779–1804.
[5] A. Cichocki, R. Zdunek, Multilayer nonnegative matrix factorization using projected gradient approaches, Int. J. Neural Syst. 17 (6) (2007) 431–446.
[6] C.I. Chang, An information theoretic-based approach to spectral variability, similarity and discriminability for hyperspectral image analysis, IEEE Trans. Inf. Theory 46 (5) (2000) 1927–1932.
[7] P.S. Chavez, S.C. Slides, J.A. Anderson, Comparison of three different methods to merge multiresolution and multispectral data: Landsat TM and SPOT panchromatic, Photogr. Eng. Remote Sens. 57 (3) (1991) 295–303.
[8] Y. Chen, Z. Xue, R.S. Blum, Theoretical analysis of an information-based quality measure for image fusion, Inf. Fus. 2 (2008) 161–175.
[9] China Centre for Resources Satellite Data and Application, http://www.cresda.com.
[10] M. Deshmukh, U. Bhosale, Image fusion and image quality assessment of fused images, Int. J. Image Process. 4 (5) (2010) 484–508.

[11] M.C. El-Mezouar, N. Taleb, K. Kpalma, J. Ronsin, An IHS-based fusion for color distortion reduction and vegetation enhancement in IKONOS imagery, IEEE Trans. Geosci. Remote Sens. 49 (5) (2011) 1590–1602.
[12] Google Map, http://ditu.google.cn/maps.
[13] G. Healey, D. Slater, Models and methods for automated material identification in hyperspectral imagery acquired under unknown illumination and atmospheric conditions, IEEE Trans. Geosci. Remote Sens. 37 (6) (1999) 2706–2717.
[14] P.O. Hoyer, Non-negative sparse coding, IEEE Workshop Neural Netw. Signal Process. (2002) 557–565.
[15] S. Jia, Y. Qian, Constrained nonnegative matrix factorization for hyperspectral unmixing, IEEE Trans. Geosci. Remote Sens. 47 (1) (2009) 161–173.
[16] N. Keshava, A survey of spectral unmixing algorithms, Lincoln Lab. J. 14 (1) (2003) 55–78.
[17] D.D. Lee, H.S. Seung, Learning the parts of objects by non-negative matrix factorization, Nature 401 (1999) 788–791.
[18] C.J. Lin, Projected gradient methods for non-negative matrix factorization, Neural Comput. 19 (10) (2007) 2756–2779.
[19] D. Manolakis, D. Marden, G.A. Shaw, Hyperspectral image processing for automatic target detection applications, Lincoln Lab. J. 14 (1) (2003) 79–116.
[20] J.M.P. Nascimento, J.M.B. Dias, Vertex component analysis: a fast algorithm to unmix hyperspectral data, IEEE Trans. Geosci. Remote Sens. 43 (4) (2005) 898–910.
[21] A. Pellemans, R. Jordans, R. Allewijn, Merging multispectral and panchromatic SPOT images with respect to the radiometric properties of the sensor, Photogr. Eng. Remote Sens. 59 (1) (1993) 81–87.
[22] W. Roberts, J.V. Aardt, F. Ahmed, Assessment of image fusion procedures using entropy, image quality, and multispectral, J. Appl. Remote Sens. 2 (2008) 023522.
[23] J.W. Roberts, J. Van Aardt, F. Ahmed, Assessment of image fusion procedures using entropy, image quality, and multispectral classification, J. Appl. Remote Sens. 1 (2008) 023522.
[24] G.A. Shaw, H.K. Burke, Spectral imaging for remote sensing, Lincoln Lab. J. 14 (1) (2003) 3–28.
[25] E.M. Schetselaar, Fusion by the IHS transform: should we use cylindrical or spherical coordinates, Int. J. Remote Sens. 19 (4) (1998) 759–765.
[26] H.Z.M. Shafri, A. Suhaili, S. Manso, The performance of Maximum likelihood spectral angle mapper neural network and decision tree classifiers in hyperspectral image analysis, J. Comput. Sci. 3 (6) (2007) 419–423.
[27] US Army Corps Engineers, http://www.tec.army.mil/hypercube/.
[28] V. Vijayaraj, C.G.O. Hara, N.H. Younan, Quality analysis of pansharpened images, Geosci. Remote Sens. Symp. (2004) 85–88.
[30] R. Zdunek, A. Cichocki, Fast nonnegative matrix factorization algorithms using projected gradient approaches for large-scale problems, Comput. Intell. Neurosci. (2008) 1–13.
[31] Y. Zhang, G. Hong, An IHS and wavelet integrated approach to improve pansharpening visual quality of natural colour IKONOS and QuickBird images, Inf. Fus. 6 (2005) 225–234.
[32] B. Zhukov, D. Oertel, F. Lanzl, G. Reinhäckel, Unmixing-based multisensor multiresolution image fusion, IEEE Trans. Geosci. Remote Sens. 37 (3) (1999) 1212–1226.